TOWARDS EFFICIENT AND TIME-ACCURATE SIMULATIONS OF EARLY STAGES OF INDUSTRIAL SCALE EXPLOSIONS

Zivkovic, D.[1*] and Sattelmayer, T.[1]
[1] Chair of Thermodynamics, Technical University of Munich (TUM), Boltzmannstraße 15, Garching, 85747, Germany, *zivkovic@td.mw.tum.de

ABSTRACT

Combustion during a nuclear reactor accident can result in pressure loads that are potentially fatal for the structural integrity of the reactor containment or its safety equipment. Enabling efficient modelling of such safety-critical scenarios is the goal of ongoing work. In this paper, attention is given to capturing early phases of flame propagation. Transient simulations that are not prohibitively expensive for use at industrial scale are required, given that a typical flame propagation study takes a large number of simulation time steps to complete. An improved numerical method used in this work is based on explicit time integration by means of Strong Stability Preserving (SSP) Runge-Kutta schemes. These allow an increased time step size for a given level of accuracy—reducing the overall computational effort. Furthermore, a wide range of flow conditions is encountered in analysis of accelerating flames: from incompressible to potentially supersonic. In contrast, numerical schemes for spatial discretization would often prove lacking in either stability or accuracy outside the intended flow regime—with density-based schemes being traditionally designed and applied to compressible (Ma>0.3) flows. In the present work, a formulation of an all-speed, density-based, numerical flux scheme is used for simulation of slow flames, starting from ignition. Validation was carried out using experiments with spherical lean hydrogen flames at laboratory scale. Turbulence conditions in the experiments correspond to those that can arise in a nuclear reactor containment during an accident. Results show that the new numerical method has the potential to predict flame speed and pressure rise at a reduced computational effort.

Keywords: hydrogen explosions, slow flames, efficient numerical simulations, CFD

1.0 INTRODUCTION

Safety concerns regarding accidental hydrogen combustion are of critical importance to a number of technical fields. In recent decades, hydrogen increasingly plays a role of an energy transport and storage medium, while traditionally, hydrogen safety has already been a major consideration in process industries and nuclear power generation. Low ignition energy of hydrogen adds to the risk of accidental (weak) ignition, which can occur at a hot surface, by a hot particle or a spark. Generally, a slow flame starts to propagate after such ignition. Acceleration of a flame can occur due to turbulence and intrinsic flame instabilities to latter of which hydrogen flames are particularly prone. In cases where the flame acceleration is strong enough, a transition to detonation can occur. Fast flames are accompanied by pressure rise and steep pressure gradients that can be detrimental to various plant structures. This makes avoiding flame acceleration an essential goal of plant safety measures. Numerical modelling focusing on early phase of flame propagation plays, in turn, an important role in design and analysis of such measures. Obstructions to flow in semi-confined spaces induce turbulence which accelerates the flame during the course of flame propagation. This makes the accurate prediction of turbulent flame speed a requirement for numerical methods in the area of nuclear safety analysis [1].

An OpenFOAM-based [2] simulation code for safety-relevant combustion was introduced by Ettner [3]. A density-based formulation allowed for accurate resolution of gas dynamics effects that are relevant to fast flames—the focus of the work being deflagration-to-detonation transition for the nuclear safety application. Applying the method to large-scale problems was accomplished by Hasslberger et al. [4] who introduced a volume-of-fluid interface tracking method to model the flame as a thin discontinuity. In nuclear safety, it is critical to consider the presence of carbon monoxide in numerous reactor accident scenarios. The work of Barfuss et al. [5] extended the aforementioned framework to hydrogen-carbon

monoxide-air mixtures. However, fast flames remained the focus of that effort. In present work, the density-based modelling framework in OpenFOAM is extended to slow flame regimes. Due to large physical scales and the need to investigate a great number of different potential accident scenarios, developments in the numerical methodology in the area of reactor safety are particularly focused on computational efficiency. This work shows that time integration methods are an area where gains in computational performance can be accomplished. Laboratory-scale, turbulent flame experiments in a spherical vessel by Goulier et al. [6, 7] investigated flame propagation in conditions that could be encountered in parts of a nuclear reactor containment during an accident. These experiments are used in present work as a source of validation data for the numerical method.

2.0 NUMERICAL METHOD

2.1 Compressible Reacting Flow Modelling

Dynamics of a compressible, reacting flow are described by unsteady Reynolds-Averaged Navier-Stokes (RANS) equations, representing conservation of mass, linear momentum, and energy. Additionally, an equation representing chemical species is required for reacting flows. Spatial discretization of the equations is realized using the finite volume method, applied to the integral form of the coupled equation set:

$$\frac{\partial}{\partial t}\int_V U_i dV + \oint_S (F_i - G_i) n_j dS = \int_V Q_i dV \tag{1}$$

where U_i is a vector conservative variables, F_i inviscid flux vector, G_i viscous flux vector, and Q_i vector of volumetric sources, each defined as

$$U_i = \begin{bmatrix} \rho \\ \rho u_i \\ \rho E \\ \rho b \end{bmatrix}, \quad F_i = \begin{bmatrix} \rho u_j \\ \rho u_i u_j + p\delta_{ij} \\ (\rho E + p)u_j \\ \rho b u_j \end{bmatrix}, \quad G_i = \begin{bmatrix} 0 \\ \sigma_{ij} + \tau_{ij} \\ u_i(\sigma_{ij} + \tau_{ij}) + \kappa_{eff}\left(\frac{\partial T}{\partial x_j}\right) \\ \rho D_{eff}\left(\frac{\partial b}{\partial x_j}\right) \end{bmatrix}, \quad Q_i = \begin{bmatrix} 0 \\ 0 \\ 0 \\ \dot{\omega} \end{bmatrix}. \tag{2}$$

Conservative variables (U_i) are defined using: ρ – density, u_i – velocity in the coordinate direction x_i, E – total energy and b – reaction progress variable—a scalar substituting chemical species, defined so that b = 1 in reactants and b = 0 in products. Furthermore, in F_i, G_i and Q_i the following quantities are found: p – pressure, T – temperature, σ_{ij} – viscous stress tensor, τ_{ij} – turbulent stress tensor, κ_{eff} – effective thermal conductivity, D_{eff} – effective diffusivity of the gas mixture, and $\dot{\omega}$ – source term of the reaction progress variable. The coupled set of equations is completed by the equation of state of a perfect gas. Furthermore, the temperature dependence of dynamic viscosity coefficient μ is calculated by Sutherland's empirical relation. The temperature dependency of specific heats is obtained from NIST-JANAF thermochemical tables. A cell-centred formulation of the finite volume method is used by means of explicit spatial discretization operators implemented in OpenFOAM [2].

In numerical simulation of compressible flow, spatial discretization of convective fluxes present in F_i is commonly accomplished with upwind schemes that consider physical properties of hyperbolic terms. When accelerating flames are analysed—starting from ignition—a wide range of flow conditions emerges, therefore a formulation that is not restricted by the Mach number is required. In present work, a flux-vector splitting scheme AUSM$^+$up (Advection Upwind Splitting Method) by Liou [8] is used. The all-speed criterion is accomplished by the pressure diffusion term, introduced for coupling between pressure and velocity at low Mach numbers. Furthermore, the numerical dissipation of the scheme is scaled proportionally to the local flow speed [8]. AUSM$^+$up scheme has been originally derived for inert gas dynamics. An extension for reacting flow was accomplished by addition of the reaction progress variable flux.

Closure models for turbulence effects are required for RANS. A scale-adapting (SAS) version of the k-ω SST turbulence model, developed by Menter and Egorov [9, 10] for unsteady simulations is applied in present work.

The combustion model

Explosion dynamics are driven by the release of thermal energy, resulting from chemical reactions. The media involved are gaseous, while the reactants can be considered premixed. Vast complexities that exist in chemistry of premixed combustion are simplified by the assumption of a single, one-step, irreversible chemical reaction—from reactant to product mixture. After the simplification, chemical reactions can be represented by a scalar quantity: the reaction progress variable [11, 12]. The transport of the Favre-averaged reaction progress variable is solved by an equation that is a part of the coupled set of RANS equations (Eq. 1).

The main goal of premixed turbulent combustion modelling is predicting the mean reaction rate—appearing as the progress variable source term in Eq. 2. A typical turbulent premixed flame occurs in conditions of high Damköhler number [13]. In this regime, the flame front thickness can be considered small, while the burning rate is proportional to the area of the flame front. Consequently, the ratio of a laminar flame speed S_L—which depends only on the unburned mixture properties and thermodynamic state—and the turbulent flame speed S_T is equal to the wrinkling of the flame front. In this work, a correlation by Dinkelacker et al. [14] is used for calculating the speed of the flame wrinkled by turbulence:

$$S_T = S_L\left(1 + \frac{0.46}{Le}Re_t^{0.25}\left(\frac{u'}{S_l}\right)^{0.3}\left(\frac{p}{p_{ref}}\right)^{0.2}\right). \quad (3)$$

Here, Re_t is the turbulent Reynolds number, u' the fluctuating component of velocity, S_L the laminar flame speed, p the pressure, Le the effective Lewis number of the mixture, and p_{ref} =1bar. In the model implementation, the local cell values are taken for all quantities except for p_{ref} which is a constant. The correlation given by Eq. 3 has been previously successfully applied to combustion problems in nuclear reactor safety by Hasslberger et al. [4] and Barfuss et al [5]. Inclusion of the Lewis number dependence in Eq. 3 is particularly important for lean mixtures (Le < 1) where flame wrinkling due to the thermal-diffusive instability is significant. Furthermore, the effects of temperature and pressure were taken into account when calculating the laminar flame speed S_L [15]:

$$S_L = S_{L,0}\left(\frac{T}{T_{ref}}\right)^{\alpha}\left(\frac{p}{p_{ref}}\right)^{\beta} \quad (4)$$

where $S_{L,0}$ is unstretched laminar flame speed at reference conditions, T and p local temperature and pressure with reference values T_{ref} =293 K and p_{ref} =1 bar. Exponents α and β, as well as $S_{L,0}$ are obtained empirically and prescribed in simulations as functions of composition, as defined in [15]. A multitude of experimental results available in the literature [16-20] were used for deriving the $S_{L,0}$ correlation [15]. Laminar flame thickness δ_L, Lewis number Le and $S_{L,0}$ of the investigated hydrogen-air mixtures can be found in Table 1.

Finally, using the progress variable gradient [21] to close the burning rate—an approach known as burning velocity model—the source term can be written as

$$\dot{\omega} = \rho_u S_t\left|\frac{\partial \tilde{b}}{\partial x_j}\right| \quad (5)$$

where ρ_u is the density of the unburnt mixture and S_T is the turbulent flame speed. Unburned density is defined as $\rho_u = p/(R_u T_u)$, where R_u is the specific gas constant of the unburned mixture, and T_u is the unburned mixture temperature, calculated by the isentropic law, using the local pressure. Use of the isentropic law is justified for validation in the slow flame regime presented in this work since the

compression of the unburned mixture near the flame front can be considered weak in deflagrations [4]. However, this approach cannot be considered general for all safety-relevant combustion and non-isentropic changes due to, e.g. shocks will need to be considered in cases where they appear. The burning velocity model in Eq. 5 was implemented within the OpenFOAM finite-volume framework by Weller [22] and Tabor and Weller [23].

2.2 Efficient Time Integration

Time-accurate numerical simulation of flame acceleration typically requires a large number of time steps to complete. The process is gradual in nature and there is a need to resolve propagating pressure waves in order to correctly represent the formation of flow discontinuities. In such conditions, time integration plays a large role in the overall computational efficiency. For long-running transient simulations, explicit time integration methods present themselves as a good choice due to their low cost per time step.

When the system of governing equations (Eq. 1) is approximated by a finite volume discretization, the resulting system of nonlinear, ordinary differential equations that can be written as

$$\frac{\Delta U_i V}{\Delta t} + R_i = 0 \tag{6}$$

where U_i is the vector of unknowns—conservative variables, V is the cell volume and R_i is the combined approximation of volume integrals of flux (F_i and G_i) and source terms (Q_i). It represents the complete spatial discretization, and it is a nonlinear function of time and the conservative variables $R_i(t, U_i)$.

The explicit time integration method used in this work belongs to the class of Strong Stability Preserving (SSP) Runge-Kutta schemes [24]. SSP methods have been designed specifically for solving systems of ordinary differential equations (ODEs) that result from spatial discretization of the hyperbolic partial differential equations containing discontinuities. It has been shown that traditional (non-SSP) methods can produce oscillatory solutions, even when the spatial discretization of the PDE system is TVD (Total Variation Diminishing) [25]. SSP methods are of the same general form and don't introduce additional cost compared to traditional Runge-Kutta methods.

In present work, a low storage implementation of a second-order SSP Runge-Kutta method by Ketchson [26] is used. Low storage methods leverage the fact that it is possible to express a Runge-Kutta method by using linear combinations of intermediate stages in such a way that storage of every stage can be avoided. Low storage methods are best analysed when written in the Shu-Osher form [25]. That way, the linear dependencies among stages become apparent. A Shu-Osher form of a general Runge-Kutta method is given by

$$\begin{aligned} &y_1 = U_i^n, \\ &y_i = \sum_{j=1}^{i-1} \left(\alpha_{ij} y_j + \beta_{ij} \Delta t R(y_j)\right) \quad 2 \le i \le m+1, \\ &U_i^{n+1} = y_{m+1} \end{aligned} \tag{7}$$

where vector y_i contains intermediate solutions for individual stages; U_i^n is the approximation at the old time level and the time step is $\Delta t = t^{n+1} - t^n$. In the second-order Ketchson [26] method used in present work, the y_i is defined as

$$y_i = \alpha_{i,1} U_i^n + \alpha_{i,i-1} y_{i-1} + \beta_{i,i-1} \Delta t R(y_{i-1}) \tag{8}$$

The number of stages can be dynamically chosen by the user, such that it provides a desired level of stability. For an m-stage method, α and β are

$$\alpha_{i,i-1} = \begin{cases} 1 & \text{if } 1 \le i \le m-1, \\ \frac{m-1}{m} & \text{if } i = m, \end{cases}$$
$$\beta_{i,i-1} = \begin{cases} \frac{1}{m-1} & \text{if } 1 \le i \le m-1, \\ \frac{1}{m} & \text{if } i = m, \end{cases} \tag{9}$$
$$\alpha_{m,0} = \frac{1}{m}.$$

3.0 NUMERICAL METHOD VALIDATION

3.1 Validation Experiments

Experiments by Goulier et al. [6, 7] were performed in a spherical vessel with an internal diameter of 563 mm (total volume of 93.43 l). The choice of hydrogen-air mixtures and turbulence intensities was made such that they represent conditions that are possible to occur in a containment during a reactor accident. Four different hydrogen-air mixtures were investigated. Those are characterized by molar concentrations of hydrogen, that were: x_{H_2}= 16, 20, 24 and 28 vol.-%, corresponding to equivalence ratios of Φ = 0.45, 0.6, 0.65 and 0.97, respectively. The maximum relative error of the equivalence ratio is reported to be 1.8%. A set of eight fans was used for turbulence generation. Instantaneous velocity field in the vessel was measured using PIV. It was established that fans generated homogeneous and isotropic turbulence within 70 mm in diameter from the centre of the vessel. Turbulence length scale varied between 43.9 mm and 52.4 mm and was dependent on blade geometry. An electric spark from two electrodes was used for ignition in the centre. Schlieren photography was used for flame position measurements, while piezoelectric transducers—flush mounted in the wall—were used for pressure. All experiments were performed at initial conditions of p = 100 kPa and T = 293 K. For each mixture-turbulence combination, ten identical trials were performed. Cases with higher turbulence show a higher scatter in experimental results of the flame position. Furthermore, mixtures with lower hydrogen content show higher scatter in the flame position than the richer mixtures. Pressure measurements, on the other hand, showed a very low standard deviation [7].

3.2 Computational Details

Two computational domains were used for simulations. The computational domain representing the whole combustion vessel is designated as Domain A in Figure 1. It consists of one-eighth of a sphere with a vessel wall modelled by no-slip boundary condition and the remaining domain boundaries as symmetries. The reduction of the domain by means of symmetry conditions was made possible by the observation that the flame shape remained spherical in the experiments within the area where measurements were taken [6, 7]. The grid was block-structured, consisting of approximately seven thousand control volumes, with spacing varying from 6 to 16 mm, while in the central area being consistently 12 mm.

The second type of the domain (Domain B in Fig. 1) was used for obtaining flame position and displacement speed results. It represents a geometric reduction of Domain A, cubic in shape, with a 120 mm side length. It models the zone of isotropic homogeneous turbulence in the experiments—where the measurements of flame position were taken—i.e. the 70 mm of the vessel radius. Non-reflective farfield boundary conditions were used for open ends of the domain. The grid of the Domain B is structured with grid spacing of 5 mm and approximately 14 thousand control volumes.

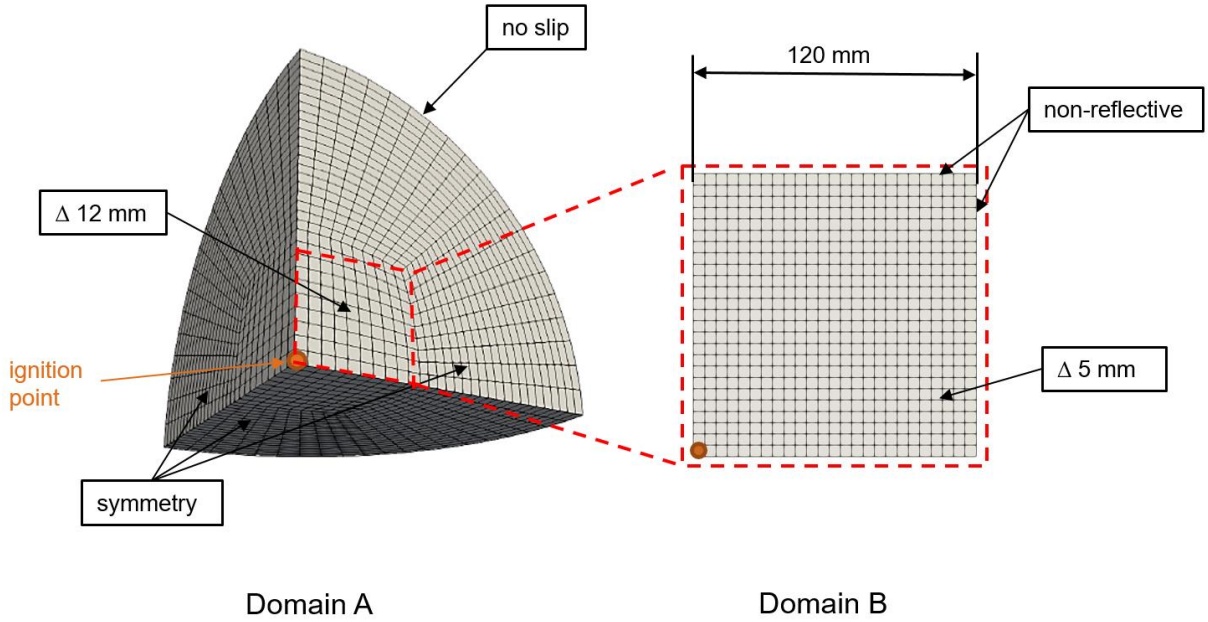

Figure 1. A view of the two computational domains used for simulations. Domain A models the whole combustion vessel, while the reduced Domain B models the area of flame position measurements.

Ignition was performed in the first time step of the simulation, by switching the progress variable to burned state (from b = 1 to b = 0). Ignition was initiated in a single control volume at the centre of the vessel, as marked in Fig. 1. Pressure and momentum diffusion coefficients of the AUSM$^+$up flux scheme were set to K_p = 0.25, and K_u = 0.75 respectively, while the limiting Mach number was set to M_{lim} = 0.6. The turbulent Prandtl and Schmidt numbers assumed unity and remained unchanged across all calculations. No tuning of those parameters was attempted. Parameters that were case-specific like CFL and number of Runge-Kutta stages (m) will be presented together with the discussion of the results.

3.3 Results and Discussion

Simulations were conducted for all four experimentally investigated H_2 mixtures (x_{H_2}=16, 20, 24, 28 vol.-%), at three levels of turbulence. Mixture-specific quantities are given in Table 1, while the turbulence quantities and root-mean-square (RMS) velocities u′ are shown in Table 2.

Table 1. Unstretched laminar flame speed at reference conditions $S_{L,0}$ [15], laminar flame thickness δ_L and Lewis number Le [15] for the investigated hydrogen-air mixtures.

x_{H_2}[%]	$S_{L,0}$ [m/s]	$\delta_L = a_u/S_{L,0}$ [mm]	Le [-]
16	0.46	0.057	0.51
20	0.85	0.032	0.63
24	1.34	0.022	0.79
28	1.87	0.016	1.02

Flame position results obtained using Domain B are shown in Fig. 2. The position of the flame is defined by the centre of the turbulent flame brush—represented by the value of b = 0.5. No adjustments of the results in time were performed. Computations were completed with CFL = 1 and m = 3. Numerical results of the flame position over time fall mostly within the standard deviation interval of the experimental results (Fig. 2). However, it can be observed that in the case of the mixture with near-stoichiometric hydrogen concentration (x_{H_2} = 28 vol.-%) and low turbulence the flame arrives at any given radius slightly later than in the experiments while for the x_{H_2} = 20 vol.-% the flame arrival time

is slightly ahead in case of the medium turbulence. The highest correspondence with experiments is for the leanest case (x_{H_2} = 16 vol.-%).

Table 2. Investigated turbulence intensity levels.

Turbulence level	u' [m/s]	Fan rpm [-]	k [m^2/s^2]	ω [1/s]
Low	0.57	1000	0.48	26.05
Medium	1.28	2000	2.44	58.78
High	2.1	3000	6.65	97.05

Furthermore, flame speed over distance is shown in Fig. 3. The flame displacement speed was obtained by differentiating the results of flame position over time. Closer to the ignition point ($\leq$ 30 mm) simulations show lower flame speeds than those in experiments. This effect is more pronounced for mixtures with higher chemical reactivity (characterized by higher laminar flame speed S_L and lower laminar flame thickness δ_L). It was observed in the simulation results that the gradient of progress variable requires a distance of several cells to fully develop in the solution field after ignition. This could cause the initial deficit of the flame speed, given that the gradient of progress variable directly determines the magnitude the burning rate (Eq. 5). In cases where x_{H_2} = 20 vol.-% and x_{H_2} = 24 vol.-% a slight overprediction of the flame speed is observed as the flame radius grows (Fig. 3). In case of the near-stoichiometric mixture with x_{H_2} = 28 vol.-% and the leanest x_{H_2} = 16 vol.-% the flame speed corresponds more closely to the experimental results and the overprediction is not pronounced. A difference in how the mixture is ignited in the experiments and modelled in simulations could potentially cause some discrepancies in the results. Namely, in the experiments, ignition energy is added to the system which is not the case in simulations where only a conversion of the chemical energy of the fuel is triggered.

Prediction of pressure gradients and peak values are of a particular importance in explosion safety analysis. Moreover, timing of the steep pressure rise corresponds with flame arrival to the vessel wall vicinity and can be a further way of assessing the prediction of turbulent flame speed. Figs. 4-6 show simulation results for pressure—obtained using Domain A—compared to the experimental data. The CFL criterion was set to unity in these simulations. The number of stages of the SST Runge-Kutta method was m = 8 to ensure stability during the steep pressure rise. Several trials with lower CFL limits (0.1, 0.3, 0.5) were conducted, showing the result to be independent of CFL. A trial with a finer grid (mesh spacing in the centre of the domain of 7 mm) was completed showing a negligible difference in the result. The maximum pressure reached in simulations is the adiabatic isochoric complete combustion pressure for a given mixture. The peak pressure in the experiments rose close to that value, but due to heat loss it remained below it. Heat transfer was not modelled in the simulations, which is why the pressure remains at the peak value after the complete combustion—in contrast to the experiment where the pressure starts to drop off at that moment.

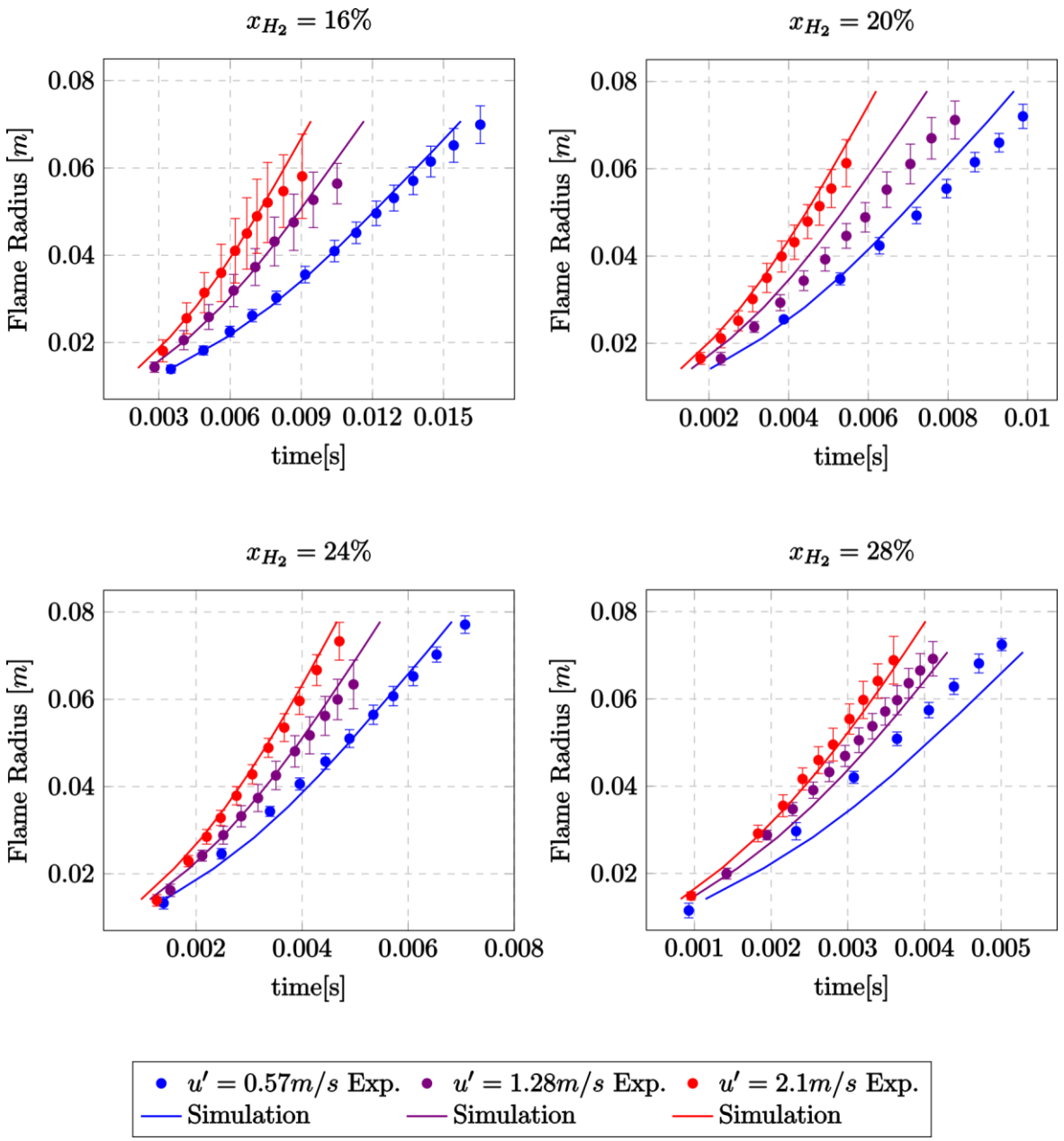

Figure 2. Flame position over time results. Computed on Domain B.

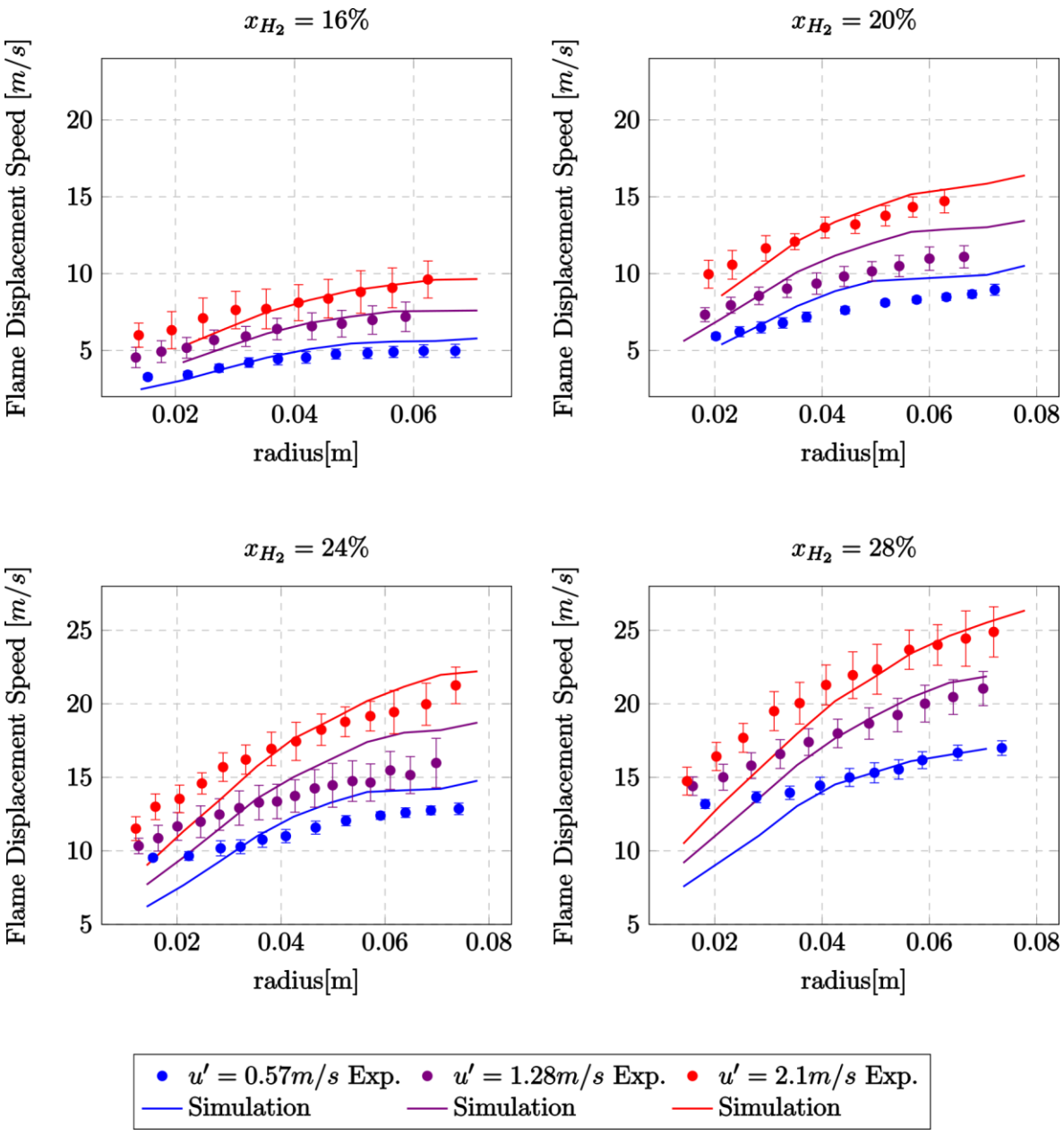

Figure 3. Flame displacement speed results. Computed on Domain B.

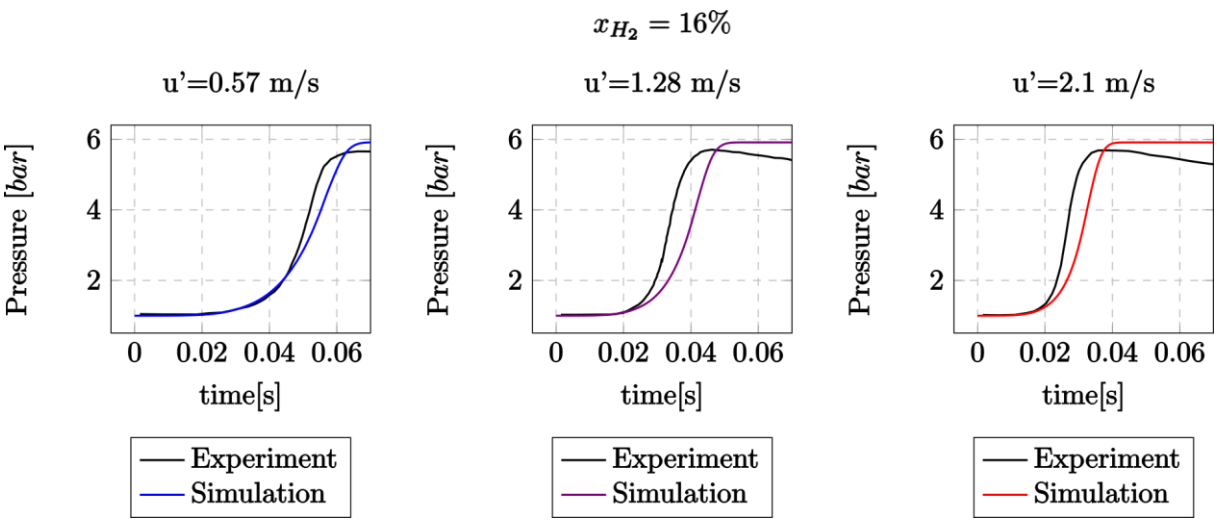

Figure 4. Pressure rise for the x_{H_2} = 16% mixture. Computed on Domain A.

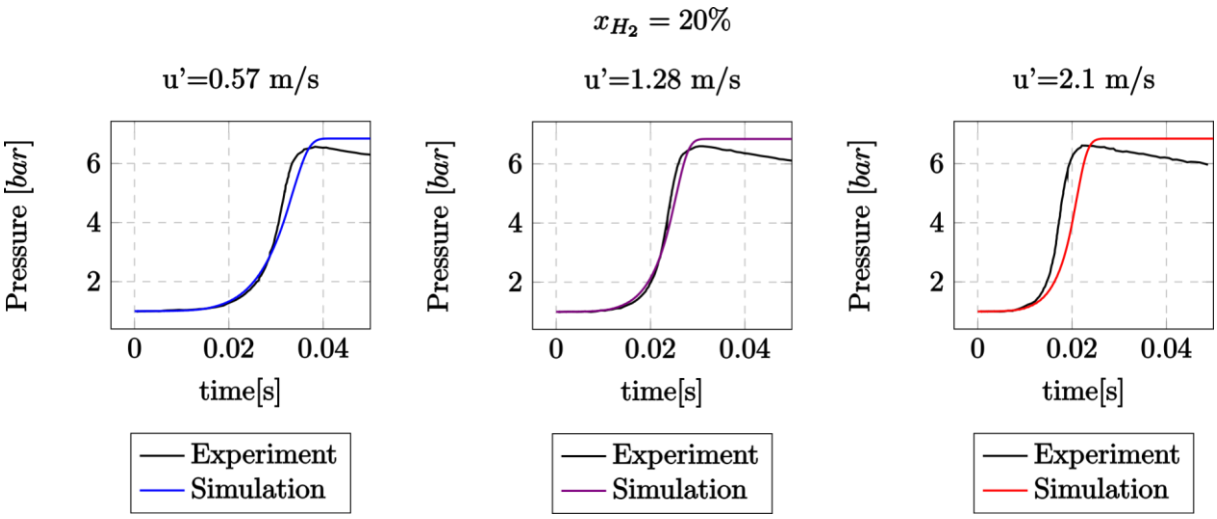

Figure 5. Pressure rise for the x_{H_2} = 20% mixture. Computed on Domain A.

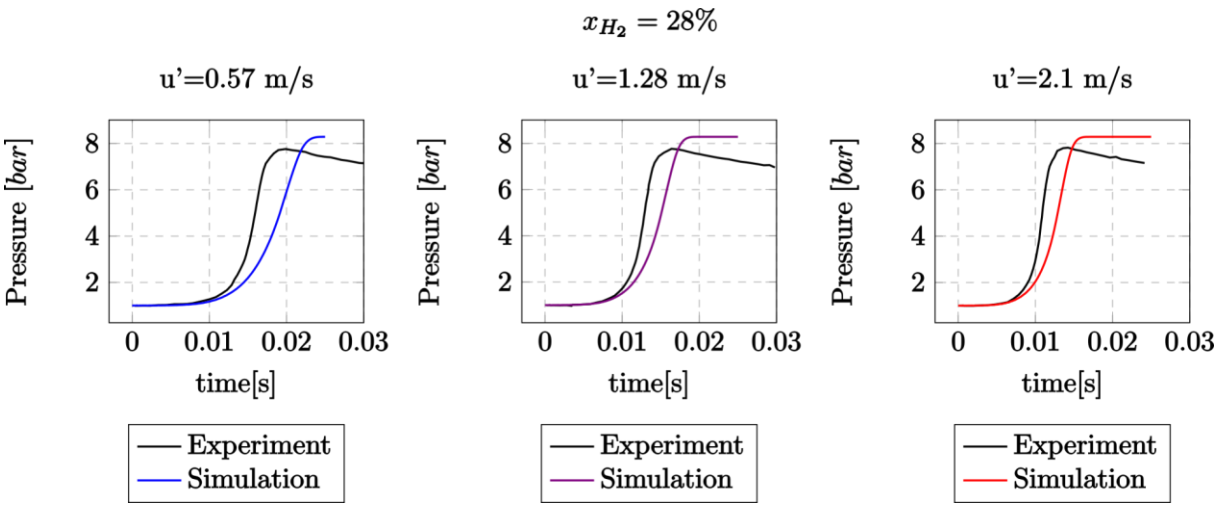

Figure 6. Pressure rise for the x_{H_2} = 28% mixture. Computed on Domain A.

Relative performance of the time integration methods is presented next. The comparison is made between a forward Euler, a conventional four-stage, second-order Runge-Kutta and an SSP Runge-Kutta method. First, computation of flame propagation using Domain B for 16 ms of simulated time is given. Performance is compared for simulations with comparable levels of accuracy (Fig. 7). The required compute time for different methods can be seen in Table 3. Multiple entries for SSP Runge-Kutta method correspond to different CFL numbers and m parameters. The m parameter can be dynamically adjusted according to the required level of stability. Both Runge-Kutta methods are able to compute the result in about a half of the computational time in contrast to the base Euler scheme. The performance gains come from a higher CFL—reducing the number of time steps for the calculation. To achieve the same stability and accuracy, the base Euler had to be run with CFL = 0.2. Despite the substantial increase in m at CFL=2 and CFL=3, the efficiency of the SSP method increased overall compared to the base Euler. However, the highest CFL doesn't result in the highest efficiency. The optimal point is closer to the CFL = 2.

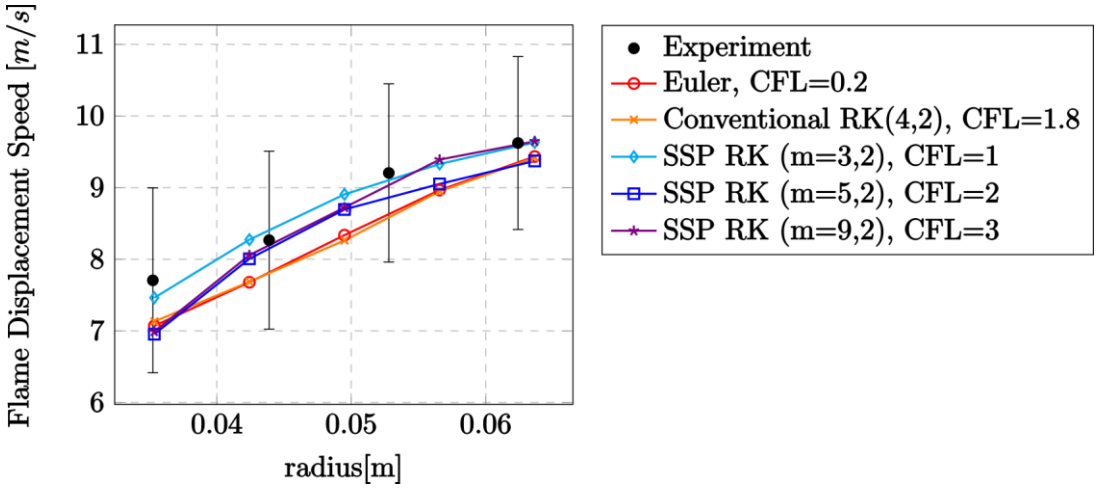

Figure 7. Results of turbulent flame speed at x_{H_2} = 16% and high level of turbulence (u' = 2.1m/s) for different time integration methods (Domain B). Each method is run at the maximum allowable CFL needed to achieve a comparable level of accuracy. The numbers in the brackets for Runge-Kutta schemes are the number of stages, and the order of the method, respectively. CPU time comparison is given in Tab. 3.

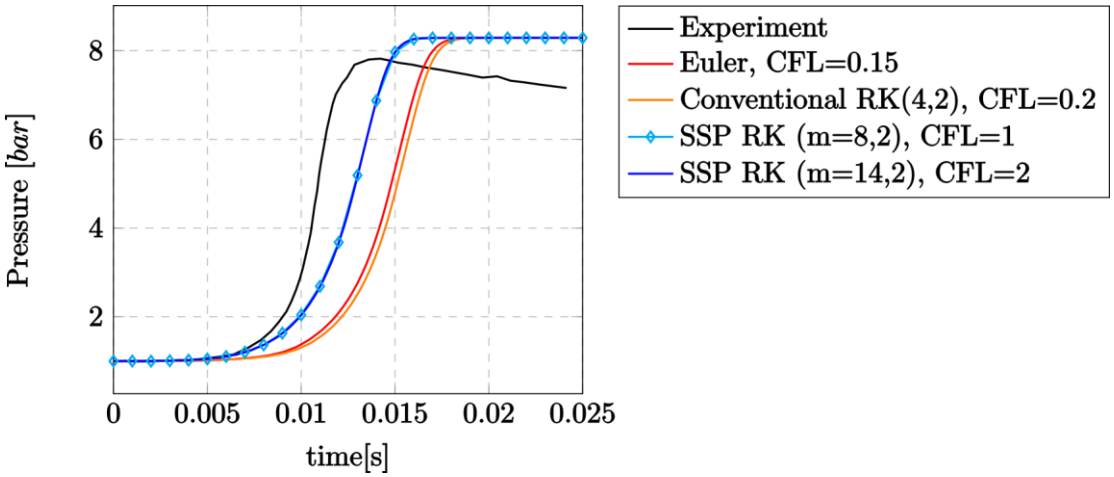

Figure 8. Results of pressure rise at x_{H_2} = 28% and high level of turbulence (u' = 2.1m/s) for different time integration methods (Domain A). CPU time comparison is given in Tab. 4.

Table 3. Time integration performance for flame propagation simulations (Domain B).

Time Integration Method	Max CFL	CPU Time
Euler	0.2	445 s
Conventional RK(4, 2)	1.8	216 s
SSP RK(m=3, 2)	1	241 s
SSP RK(m=5, 2)	2	190 s
SSP RK(m=9, 2)	3	223 s

Performance of the time integration is assessed again using simulations of flame propagation and pressure rise obtained using Domain A for 25 ms of simulated time. Compute times with different methods can be seen in Table 4. Here the goal of making a comparison of efficiency at a comparable level of accuracy was pursued again. However, the result on Fig. 8 shows that forward Euler and conventional Runge-Kutta show a delay in the pressure rise compared to the SSP Runge-Kutta scheme. It persisted regardless of the CFL or mesh fineness. Furthermore, the maximum CFL for Euler and conventional Runge-Kutta schemes was severely limited by stability.

Table 4. Time integration performance for pressure rise simulations (Domain A).

Time Integration Method	Max CFL	CPU Time
Euler	0.15	665 s
Conventional RK(4, 2)	0.2	1324 s
SSP RK(m=8, 2)	1	488 s
SSP RK(m=14, 2)	2	442 s

The results show that the stability limit of a conventional RK is not significantly higher than the one for the Euler scheme. When limited by a relatively low, stability-bound CFL, a conventional four-stage method takes longer to compute than a simple forward Euler due to the higher number of stages which do not bring a benefit. On the other hand, the SSP RK with m = 14 and CFL = 2 computes the result in the shortest time, however the improvement to the CFL = 1 and m = 8 run is not dramatic. All presented calculations were done in parallel, using 4 processors on a desktop PC (AMD Ryzen 7/2700).

4.0 CONCLUSION

A density-based numerical method for efficient flame propagation simulations, capable in the slow flame regime, was presented. It is based on explicit time integration with Strong Stability Preserving (SSP) Runge-Kutta method, which is shown to improve efficiency of transient simulations by enabling a stable computation at an increased time step size. Furthermore, the SSP method allows increase in stability for cases where conventional methods are limited more strongly by the allowable CFL condition, e.g. when steep pressure gradients occur. It has been showed that the adjustable parameter of the scheme—the number of stages (m)—can be used to increase stability when necessary, or otherwise be set for optimal efficiency. An adaptive algorithm for finding optimal values of the parameter m during simulation run time would further improve the method. Spatial discretisation using a formulation of a high-resolution upwind scheme for all speeds ($AUSM^{+}up$) that was extended to reacting flows, has been proven capable of simulating slow flame propagation regimes. A particular focus in the present work has been capturing the early phase of the flame propagation, as well as the pressure rise occurring in the confined volume of the laboratory-scale combustion vessel. Results of the validation show that the numerical method presented here reproduces the flame propagation and pressure rise well for the intended use. To achieve the further goal of applicability at industrial scales additional validation of turbulent flame propagation is required at increasingly larger volumes and within semi-confined, obstacle-laden geometries.

ACKNOWLEDGMENTS

This project is funded by the German Federal Ministry of Economics and Technology (BMWi) on the basis of a decision by the German Bundestag (project no. 1501573) which is gratefully acknowledged.

REFERENCES

1. Bentaib, A., Bleyer, A., Meynet, N., et al., SARNET hydrogen deflagration benchmarks: Main outcomes and conclusions, *Annals of Nuclear Energy*, **74**, 2014, pp. 143–152.

2. Weller, H.G., Tabor, G., Jasak, H., and Fureby, C., A tensorial approach to computational continuum mechanics using object-oriented techniques, *Computers in physics*, **12**, No. 6, 1998, pp. 620–631.

3. Ettner, F., Vollmer, K.G., and Sattelmayer, T., Numerical simulation of the deflagration-to-detonation transition in inhomogeneous mixtures, *Journal of Combustion*, **2014**, 2014.

4. Hasslberger, J., Katzy, P., Boeck, L.R., and Sattelmayer, T., Computational Fluid Dynamics Simulation of Deflagration-to-Detonation Transition in a Full-Scale Konvoi-Type Pressurized Water Reactor, *Journal of Nuclear Engineering and Radiation Science*, **3**, No. 4, 2017.

5. Barfuss, C., Heilbronn, D., and Sattelmayer, T., Simulation of Deflagration-to-Detonation Transition of Lean H2-CO-Air Mixtures in Obstructed Channels, *International Conference on Hydrogen Safety*, 2019, pp.12.

6. Goulier, J., Chaumeix, N., Halter, F., Meynet, N., and Bentaïb, A., Experimental study of laminar and turbulent flame speed of a spherical flame in a fan-stirred closed vessel for hydrogen safety application, *Nuclear Engineering and Design*, **312**, 2017, pp. 214–227.

7. Goulier, J., Comandini, A., Halter, F., and Chaumeix, N., Experimental study on turbulent expanding flames of lean hydrogen/air mixtures, *Proceedings of the Combustion Institute*, **36**, No. 2, 2017, pp. 2823–2832.

8. Liou, M.-S., A sequel to AUSM, Part II: AUSM+-up for all speeds, *Journal of Computational Physics*, **214**, No. 1, 2006, pp. 137–170.

9. Menter, F.R., and Egorov, Y., The Scale-Adaptive Simulation Method for Unsteady Turbulent Flow Predictions. Part 1: Theory and Model Description, *Flow, Turbulence and Combustion*, **85**, No. 1, 2010, pp. 113–138.

10. Egorov, Y., and Menter, F., Development and Application of SST-SAS Turbulence Model in the DESIDER Project, (Peng, S.-H. and Haase, W., Eds.), 2008, Berlin, Heidelberg, pp. 261–270.

11. Bray, K., and Moss, J.B., A unified statistical model of the premixed turbulent flame, *Acta Astronautica*, **4**, No. 3–4, 1977, pp. 291–319.

12. Bray, K., and Libby, P.A., Passage times and flamelet crossing frequencies in premixed turbulent combustion, *Combustion Science and Technology*, **47**, No. 5–6, 1986, pp. 253–274.

13. Poinsot, T., and Veynante, D., Theoretical and numerical combustion, 2005, RT Edwards, Inc.

14. Dinkelacker, F., Manickam, B., and Muppala, S., Modelling and simulation of lean premixed turbulent methane/hydrogen/air flames with an effective Lewis number approach, *Combustion and Flame*, **158**, No. 9, 2011, pp. 1742–1749.

15. Katzy, P., Combustion Model for the Computation of Flame Propagation in Lean Hydrogen-Air Mixtures at Low Turbulence, PhD Thesis, Technical University Munich, Garching, 2021.

16. Dowdy, D.R., Smith, D.B., Taylor, S.C., and Williams, A., The use of expanding spherical flames to determine burning velocities and stretch effects in hydrogen/air mixtures, Elsevier 1991, pp.325–332.

17. Kwon, O., and Faeth, G., Flame/stretch interactions of premixed hydrogen-fueled flames: measurements and predictions, *Combustion and Flame*, **124**, No. 4, 2001, pp. 590–610.

18. Tse, S.D., Zhu, D., and Law, C.K., Morphology and burning rates of expanding spherical flames in H2/O2/inert mixtures up to 60 atmospheres, *Proceedings of the combustion institute*, **28**, No. 2, 2000, pp. 1793–1800.

19. Vagelopoulos, C.M., Egolfopoulos, F.N., and Law, C.K., Further considerations on the determination of laminar flame speeds with the counterflow twin-flame technique, *Symposium (International) on Combustion*, **25**, No. 1, 1994, pp. 1341–1347.

20. Wu, C.K., and Law, C.K., On the determination of laminar flame speeds from stretched flames, *Symposium (International) on Combustion*, **20**, No. 1, 1985, pp. 1941–1949.

21. Lipatnikov, A., Fundamentals of premixed turbulent combustion, 2012, CRC Press.

22. Weller, H., The development of a new flame area combustion model using conditional averaging, *Thermo-fluids section report TF*, **9307**, 1993.

23. Tabor, G., and Weller, H.G., Large Eddy Simulation of Premixed Turbulent Combustion Using Flame Surface Wrinkling Model, *Flow, Turbulence and Combustion formerly `Applied Scientific Research'*, **72**, No. 1, 2004, pp. 1–28.

24. Gottlieb, S., Ketcheson, D.I., and Shu, C.-W., Strong stability preserving Runge-Kutta and multistep time discretizations, 2011, World Scientific.

25. Shu, C.-W., and Osher, S., Efficient implementation of essentially non-oscillatory shock-capturing schemes, *Journal of computational physics*, **77**, No. 2, 1988, pp. 439–471.

26. Ketcheson, D.I., Runge-Kutta methods with minimum storage implementations, *Journal of Computational Physics*, **229**, No. 5, 2010, pp. 1763–1773.